PROGRESS TOWARD EVALUATING ROUGHNESS-RESOLVED AEROTHERMODYNAMIC SIMULATIONS FOR THE MARS SAMPLE RETURN EARTH ENTRY SYSTEM

Alireza Mazaheri[*] *and Christopher Johnston*[†]

Aerothermodynamics Branch,
NASA Langley Research Center,
Hampton, Virginia 23681

Grant Palmer [‡]

Aerothermodynamics Branch,
AMA Inc. at NASA Ames Research Center,
Moffett Field, California 94035

ABSTRACT

This work pursues the efficient Navier-Stokes simulation, using NASA's standard LAURA and DPLR simulation tools, of the flowfield and convective heating resulting from the patterned-roughness surface of the Mars Sample Return (MSR) Earth Entry System (EES). This type of simulation has been infeasible for past NASA missions. However, for EES, the combination of a patterned roughness heatshield approximated with a sinusoidal pattern, the zero degrees angle of attack nominal flow, and the supersonic boundary layer edge Mach number, all combine to make these roughness-resolved grid simulations feasible. The patterned roughness and zero degrees angle of attack nominal flow allow the simulation domain to be reduced to a thin axial flowfield slice that captures a minimum of single period of the roughness pattern. With a periodic boundary condition applied along the boundaries of this slice, simulation on the reduced domain is identical to the full domain but with significant cost saving. The supersonic boundary layer edge Mach number prevents the upstream influence, which allows the smooth stagnation region to be frozen. This freezing of the stagnation region flow is required because of the numerical instability resulting from the tight spacing of the grid in the axial direction as the stagnation point is approached. Applying the developed analysis approach to a peak heating EES case results in a roughness augmentation factor for the convective heating of 1.32, which agrees well with correlations that predict values between 1.30 and 1.37. Analysis approach developed in this work provides the framework for future studies of turbulence modeling impacts and the influence of an ablating surface.

1. INTRODUCTION

The roughness of a hypersonic entry vehicle surface may have a large impact on the convective heating to that surface [1]. This roughness augmentation of the convective heating is typically evaluated through experimentally-based correlations derived as a function of $k^+ = k(\tau_w/\rho_w)^{1/2}\rho_w/\mu_w$, where k is the roughness height, τ_w is the wall shear stress, and ρ_w and μ_w are, respectively, density and viscosity evaluated at the surface. Two widely used correlations are presented in Fig. 1, which compares the Powars [2] and Dahm [3] correlations. These provide a greater than 1.0 correction factor for the smooth wall CFD convective heating predictions, which results in the roughness-augmented convective heating. Note that the details of the rough surface are only captured in k^+ through k, which is the equivalent to a sand grain roughness height. However, because the equivalent sand grain roughness height is usually lower than the physical peak-to-valley roughness height [4], the physical value is often used to ensure conservatism is the resulting roughness augmentation factor.

The dependence of this roughness augmentation approach on only k^+ represents a necessary simplification for an experimentally-based correlation. This approach allows a wide range of experimental conditions and roughness patterns to be used to inform a given flight vehicle case, with the caveat that the experiment most similar to the flight case (beyond matching k^+) should carry more weight in the assessment, and that this measurement is sufficiently similar to the flight case to be relevant. Although there is no rigorous approach for establishing similarity between the measurement and flight case, often a range of boundary layer parameters are compared, such as the roughness height divided by boundary layer thickness (k/δ), boundary-layer momentum-thickness-based Reynolds number (Re_θ), Mach number at the boundary layer edge (M_e), or Mach number at the roughness height (M_k). The impact of boundary layer chemistry and blowing of ablation products, which are likely present for the flight case but not the measurement, are typically ignored in the similarity assessment. For flight cases, where the boundary layer parameters are notably different than available measurements or the impact of blowing or chemistry is strong, further experimental or computational studies are required to validate the roughness augmentation model.

One such flight case that matches this description of having insufficient validation data is the Mars Sample Return

[*] ali.r.mazaheri@nasa.gov
[†] christopher.o.johnston@nasa.gov
[‡] grant.e.palmer@nasa.gov

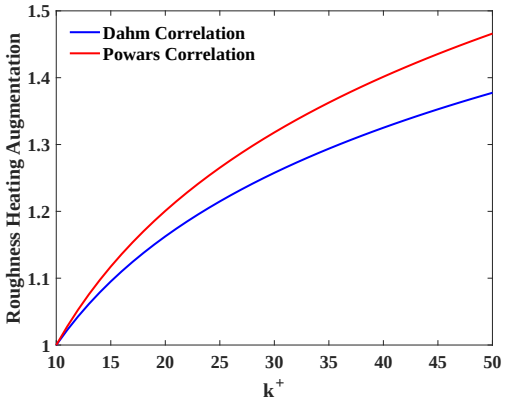

Fig. 1. Correlations for the roughness augmentation of convective heating.

(MSR) Earth Entry System (EES), which is currently being designed. This vehicle consists of a 45 degree sphere cone with nose radius of 0.3 m and maximum diameter of 1.25 m. The entry velocity is ≈12 km/s with a relatively shallow entry flight path angle of roughly -22 degrees. Figure 2 shows that this trajectory results in the EES maintaining higher velocities at lower altitudes than, for example, Stardust or Hayabusa. This higher entry velocity results in a larger impact of turbulence and roughness for EES.

Based on the Powars correlation [2], the nominal k value of 0.7 mm results in up to a 35% increase in the convective heating on the flank region of the vehicle near peak heating. While it is beyond the scope of this paper to assess the relevance of existing roughness augmentation data to EES, the primary deficiency of the existing measurements is that they do not match the high boundary layer edge Mach number, M_e predicted for EES, which is above 2.0 over much of the flank. This high M_e for EES results in a supersonic Mach number being maintained down to below the 0.7 mm roughness height, according to the smooth wall CFD simulations. The threat that the interaction of this potentially supersonic flow with the roughness elements will cause shocks to form around the roughness elements, which could result in heating and shear augmentation above that predicted by the correlations, must be addressed. Furthermore, the impact of flowfield chemistry and ablation is large for EES, which as mentioned previously, is not captured by available experiments.

These factors motivated the pursuit of simulating the EES roughness elements using NASA's standard aerothermodynamic CFD codes LAURA [5] and DPLR [6], with the goal of simulating the roughness augmentation at EES flight conditions with flight relevant chemistry (and ablation, in future work) modeled. The simulation approach developed for this analysis is presented in Section 2. Section 3 provides an example result from these simulations, which demonstrates their potential for informing the EES aerothermal environment. Section 4 then discusses the conclusions and future work.

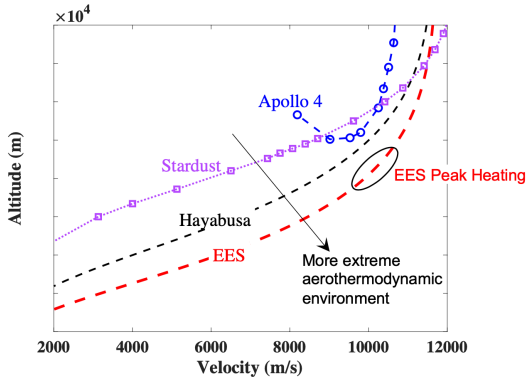

Fig. 2. Comparison of the EES trajectory with other Earth entries above 10 km/s.

2. SIMULATION APPROACH

The present roughness-resolved grid simulations are feasible because of three geometric simplifications provided by EES. The first simplification is that EES's patterned roughness may be approximated with a sinusoidal pattern with length dimensions on the order of 2 mm, which is not excessively small relative to sand grain roughness, for example. The forebody thermal protection system material for EES is Three-dimensional Medium Density Carbon Phenolic (3MDCP), which is a variant of the Heatshield for Extreme Entry Environment Technology (HEEET) material. As shown by Wilder and Prabhu [7], arc jet tests of this material at EES-relevant conditions result in a charred surface that may be represented by a sinusoidal function as:

$$z = \frac{k}{2} sin\left(\frac{\pi x}{D}\right) sin\left(\frac{\pi y}{D}\right) \quad (1)$$

where z is the height above the smooth TPS surface, x and y are the distances along the surface, k is the peak-to-valley height, and D is the peak-to-valley spacing. Wilder and Prabhu [7] show that k values of approximately 0.7 mm with D/k of 3.2. An example of this simplified pattern is presented in Fig. 3.

The second simplification provided by EES that makes the roughness-resolved grid simulations feasible is EES's zero degrees nominal angle of attack. This results in an axisymmetric nominal flowfield for the smooth wall case but not for the rough surface. For simulating the rough surface, the simplified pattern represented by Eq. (1) may be simulated over a thin slice that includes at least a single period of the roughness pattern. This flowfield slice is shown in Fig. 3, which demonstrates a slice with two periods of roughness. The sinusoidal roughness pattern allows a periodic boundary condition to be applied to the sides of these flowfield slices, which

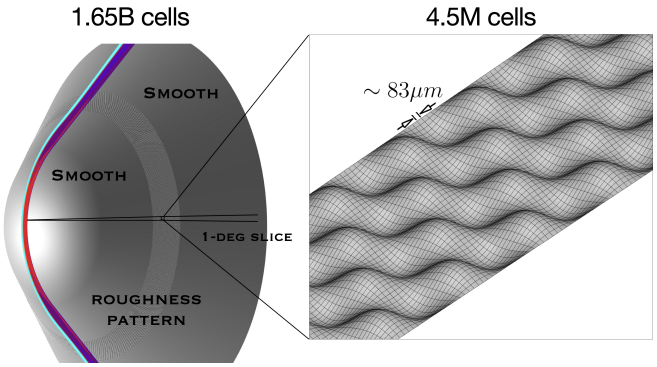

Fig. 3. Overview of the surface grid layout, which demonstrates the axial slice used for the simulations.

results in a simulation over a single period of roughness to be identical to the full domain simulation. This reduction of the simulation domain to a single period of roughness makes the present roughness-resolved grid simulations feasible. As shown in Fig. 3, over a three order-of-magnitude decrease in the number of grid cells achieved by simulating the flowfield slice relative to a half or full body simulation, with no loss in accuracy because the periodic boundary condition is exact for this roughness geometry.

The third simplification provided by EES is the supersonic M_e on the flank of the vehicle, which allows the flank region to be simulated while keeping the stagnation region flowfield frozen to the smooth wall result. The reason for needing this capability is discussed in the remainder of this paragraph. A challenge that remains in simulating the roughness-resolved grid flowfield slice shown in Fig. 3 is the propagation of the $\approx$60 grid points that span the axial direction between the two periodic boundary conditions. The spacing between these grid points reduces to zero at the stagnation point. Even if the grid is manipulated to avoid the stagnation point singularity, both LAURA and DPLR result in significant errors in the stagnation region due to this tight grid spacing, which propagates downstream to produce an unacceptable flowfield over the roughness elements. This flank region is where the roughness augmentation is the highest (according to correlations), and is therefore the target of the present simulations. The surface grid over the spherical cap of the vehicle is maintained as smooth, although the tight grid spacing in the axial direction still must be carried down to the stagnation point. The smooth stagnation region may, therefore, be obtained from a conventional axisymmetric flowfield simulation with a single grid point in the axial direction, or a coarse grid half body solution. This observation led to the development of a reconstruction tool that interpolates a converged three-dimensional flowfield solution from a standard smooth wall grid, onto the three-dimensional roughness-resolved grid slice. The interpolation of the smooth wall (coarse grid) solution onto the roughness-resolved grid is beneficial in two ways. The first is that it provides a good initialization of the flowfield over the rough surface, which helps convergence, as well as providing the shock-aligned volume grid. This volume grid from the smooth wall interpolated onto the rough surface, using the *Radial Interp* code [8], allows for grid adaptations on the rough surface grid to be avoided, which would lead to a wavy grid through the shock and outer boundary. The second benefit of this interpolated flowfield solution is that it allows the stagnation region flowfield to remain frozen during the simulation of the downstream roughness regions. The supersonic M_e values along the flank of the EES prevents upstream influence, making the frozen stagnation region approach well posed. This is achieved in LAURA and DPLR by flagging grid blocks in the stagnation region to act like a Dirichlet boundary condition.

To demonstrate the validity of the interpolation and stagnation region freezing approaches, an EES case near peak heating is simulated for a smooth wall case on a grid slice with the same resolution as the roughness resolved cases. The freestream conditions for this case are 9.8 km/s, 1.1×10^{-3} kg/m^3, and 262 K. Two-temperature thermochemical nonequilibrium is assumed with 11 species air. The flow is assumed to be fully turbulent using the Spalart-Allmaras model [9]. The Spalart-Allmaras model is chosen over the Cebeci-Smith algebraic model, which is widely used for smooth forebody aerothermal simulations, to better capture the flow details around the roughness elements. Figure 4 compares the conventional coarse grid result with the fine grid result, where the fine grid represents the roughness resolved grid with the roughness heights set to zero. Recall that this fine grid result is obtained by interpolating the coarse grid result onto the high-resolution grid slice, and then recomputing the flow with the stagnation region frozen. This figure shows that this high-resolution grid solution is able to maintain the coarse grid solution, which demonstrates that the developed reconstruction process and the stagnation region freezing approach enable solutions on this high-resolution grid. The next section will apply the same approach, but with nonzero roughness heights.

3. RESULTS

Figure 5 presents the roughness resolved grid simulations for the nominal EES k value of 0.7 mm. Axial slices that pass between and over the peaks are presented in this figure. While over a factor of two increase in the convective heating is seen at the roughness peaks, the valleys and regions between the peaks result in significantly lower heating than the smooth wall result. To convert this strongly varying heating into a useful result, averaged values over the surface are evaluated. To compute the roughness augmentation factor, which would be applied to a smooth wall solution to recover the same roughness-resolved grid heating (per unit area of the smooth wall), is presented here as two components. The first component captures the ratio of the wetted area averaged

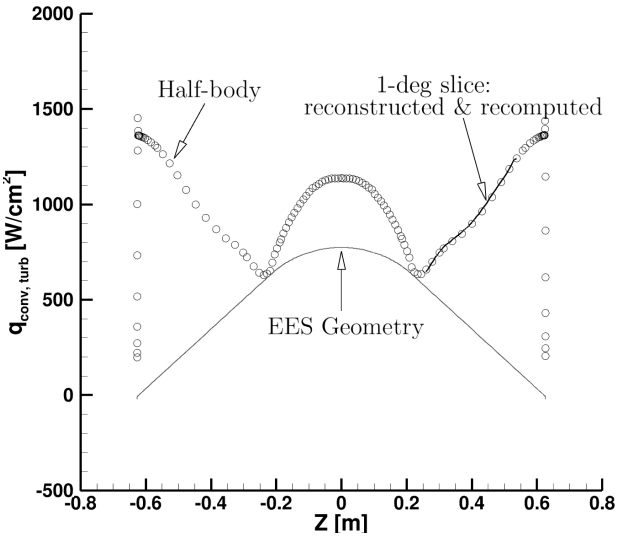

(a) Surface convective heating

Fig. 4. Verification study: comparisons between solutions predicted on a one-degree slice through the developed reconstruction technique and the three-dimensional periodic boundary condition, and the ones obtained on a typical half body surface.

heating:

$$R_1 = \frac{\int q_r dA_r}{\int dA_r} \frac{\int dA_s}{\int q_s dA_s}, \tag{2}$$

where subscripts r and s denote rough and smooth surfaces, respectively.

For the result presented in Fig. 5, the resulting R_1 is 0.96, which indicates that the decreased heating components have a slightly larger impact than the increased heating on the peaks. The second component of the roughness augmentation factor accounts for the roughness case having a larger surface area than the smooth wall case. This means that the averaged heating for the rough wall case is applied over a larger surface area than the smooth wall case, and therefore, more energy is directed into the TPS. This correction factor is written as:

$$R_2 = \frac{\int dA_r}{\int dA_s}. \tag{3}$$

For the result presented in Fig. 5, the resulting R_2 is 1.39. To be clear, this value suggests that the wetted area of the rough surface is 39% larger than the smooth surface.

Since R_1 represents the area averaged augmentation factor, the product of R_1 and R_2 represents appropriate augmentation energy factor for application to smooth wall heating. This final augmentation factor is therefore:

$$R_{\text{final}} = R_1 R_2 = \frac{\int q_r dA_r}{\int q_s dA_s}. \tag{4}$$

This augmentation factor ensures that the energy directed into the surface for the rough wall case, per unit area of the smooth wall solution, is recovered. Matching this energy component is considered not only conservative, but also the most appropriate assumption for application to material response simulations for TPS sizing. For example, a one-dimensional material response computation assumes the provided convective heating is the energy per-unit area of the smooth wall, which is obtained from the product $q_s R_{\text{final}}$, whereas using R_1 instead of R_{final} would underpredict the heating. For the present case, R_{final} is equal to 1.32. Based on the smooth wall solution along the surface region currently being simulated with roughness, the k^+ value is ≈35, which results in augmentation factors of 1.30 from the Dahm [3] correlation and 1.37 from the Powars correlation [2]. The agreement of the current value of 1.32 with these values is encouraging.

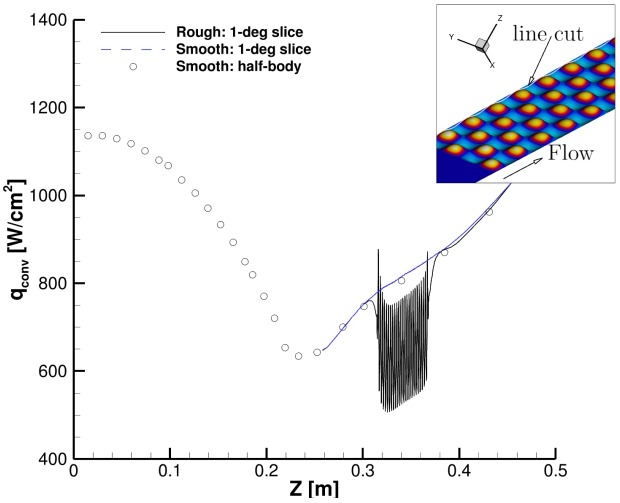

(a) Surface heat flux between the bumps

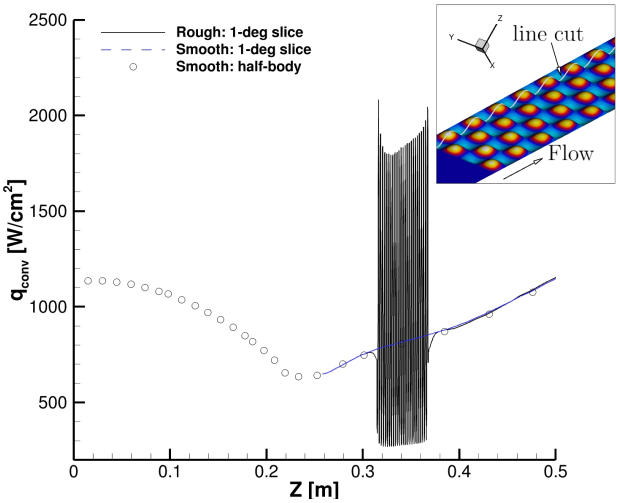

(b) Surface heat flux over the bumps

Fig. 5. Predicted convective heating for EES at the peak heating condition using the SA-Catris [9] turbulence model.

To further demonstrate the value of this simulation ap-

proach, a roughness pattern obtained using Eq. (1), but with values below $z = 0$ set to zero, was simulated as a "no-valley" case. Furthermore, the k applied to this equation was doubled so that the same peak to value height of 0.7 mm was achieved. Because the valleys were removed but the peaks doubled in height, this case has the same k^+ as the previous case. The resulting values of R_1 and R_2 are 1.24 and 1.53, respectively, which combine for an R_{final} of 1.90. Therefore, this case would be significantly underpredicted by the Powars or Dahm correlations, which remain at 1.37 and 1.30, respectively. This shows the limitations of correlations that are functions of only k^+, and further emphasizes the value of the present simulations. Fortunately for EES, this no-valley case with 0.7 mm peaks is not expected, however the no-valley case with 0.35 mm peaks may be relevant, since it is the same pattern shown in Fig. 5 but with the valleys removed. Simulations of this case result in R_1 and R_2 values of 1.09 and 1.13, respectively, which combine for an R_{final} of 1.23. This 1.23 is relatively close to the 1.32 evaluated for the nominal pattern, although the R_1 and R_2 components are noticeably different. This indicates that the character of the roughness pattern is important, along with the roughness height.

4. CONCLUSIONS AND FUTURE WORK

The present analysis is a work in progress, although a few conclusions are apparent already. The main conclusion being that a well-behaved reacting flow Navier-Stokes solution may be obtained over a realistic roughness pattern at flight relevant conditions for the Mars Sample Return (MSR) Earth Entry System (EES). To the authors' knowledge, this type of solution has not been available in the past. The EES axisymmetric smooth geometry, patterned roughness, and supersonic M_e are all required to make these simulations feasible. Using the Spalart-Allmaras Catris-Aupoix turbulence model [9] and the best estimate of the EES roughness pattern, the resulting simulations predict a roughness augmentation factor of 1.32, which is in-family with the roughness correlations applied for design. Variations in the roughness pattern around this nominal show the benefit of being able to simulate the roughness directly. Future work will investigate the sensitivity to turbulence modeling, consider grid resolution, provide comparisons with Wilder and Prabhu [7] measurements, and investigate the impact of an ablating wall. The first three of these issues need to be addressed before the results of these simulations are considered sufficient to inform EES design.

5. REFERENCES

[1] B.R. Hollis, "Experimental investigation of roughness effects on transition onset and turbulent heating augmentation on a hemisphere at Mach 6 and Mach 10," *NASA TP-2017-219613*, 2017.

[2] C.A. Powars, "Surface roughness effects on reentry heating," *Aerotherm Tech Memo 71-10*, 1971.

[3] T.J. Dahm, "Passive nosetip technology (PANT II) program," *SAMSO-TR 77-11*, 1976.

[4] R.B. Dirling, "A method for computing rough wall heat transfer rates on reentry nosetip," 1973, AIAA Paper 1973–763.

[5] K.B. Thompson, B.R. Hollis, C.O. Johnston, B. Kleb, V.L. Lessard, and A. Mazaheri, "LAURA users manual: 5.6," Tech. Rep. NASA/TM–2020–220566, NASA, February 2020.

[6] M.J. Wright, T. White, and N. Mangini, "Data parallel line relaxation (DPLR) code user manual," Tech. Rep. TM–2009–215388, NASA, October 2009.

[7] M.C. Wilder and D.K. Prabhu, "Rough wall turbulent heat transfer experiments in hypersonic free flight," 2019, AIAA Paper 2019–3009.

[8] D. Saunders, "CFD utilities (https://sourceforge.net/projects/cfdutilities)," .

[9] S. Catris and B. Aupoix, "Density corrections for turbulence models," *Aerospace Science and Technology*, vol. 4, pp. 1–11, 2000.